Molecular Crystals and Liquid Crystals Incorporating Nonlinear Optics

Publication details, including instructions for authors and subscription information:
http://www.tandfonline.com/loi/gmcl17

Ferroelectric Liquid Crystals

Robert Blinc [a] , Cene Filipič [a] , Adrijan Levstik [a] , BošTjan Žekš [a] & T. Carlsson [b]

[a] Jožef Stefan Institute, Edvard Kardelj University of Ljubljana, Jamova 39, 61111, Ljubljana, Yugoslavia

[b] Institute of Theoretical Physics, Chalmers University of Technology, S-41296, Göteborg, Sweden

Version of record first published: 17 Oct 2011.

To cite this article: Robert Blinc , Cene Filipič , Adrijan Levstik , BošTjan Žekš & T. Carlsson (1987): Ferroelectric Liquid Crystals, Molecular Crystals and Liquid Crystals Incorporating Nonlinear Optics, 151:1, 1-46

To link to this article: http://dx.doi.org/10.1080/00268948708075318

Mol. Cryst. Liq. Cryst., 1987, Vol. 151, pp. 1-46
Photocopying permitted by license only

Printed in the United States of America

FERROELECTRIC LIQUID CRYSTALS

ROBERT BLINC, CENE FILIPIČ, ADRIJAN LEVSTIK, BOŠTJAN ŽEKŠ

Jožef Stefan Institute, Edvard Kardelj University of Ljubljana, Jamova 39, 61111 Ljubljana, Yugoslavia

T. CARLSSON

Institute of Theoretical Physics, Chalmers University of Technology, S–41296 Göteborg, Sweden

Abstract The main advances in the field of bulk ferroelectric liquid crystals since 1984 are reviewed. Recent experiments have shown that the molecular tilt and the in-plane spontaneous polarization are not strictly proportional to each other as assumed before. Microscopic experiments such as NMR and NQR have further allowed for a determination of the basic order parameters as a function of the nuclear position along the molecule without unwinding the chiral helix.

I. INTRODUCTION

Ferroelectric Sm C* type liquid crystals[1,2] are orientationally ordered liquids with a one dimensional density modulation. The periodicity of the helicoidal orientational ordering and the associated helicoidal polarization is incommensurate to the periodicity of the one–dimensional density modulation.

Here we wish – after a short introduction and symmetry considerations – to review the main advances in this field since 1984 as far as bulk systems are concerned. They can be summarized as follows:

i) Much better experiments on the macroscopic as well as on the microscopic level have showed that the two basic order parameters of ferroelectric liquid crystals, i.e. the *tilt* of the molecules with respect to the normal to the smectic layers, and the *in-plane spontaneous polarization* are *not* strictly proportional to each other[3] as assumed before[1,2]. This allows for a discrimination between several theoretical models proposed so far.

NMR and NQR measurements have also allowed for a determination of the biasing of the rotation around the long molecular axis as a function of the position of the nucleus in the molecule. These data showed that the rotation of the central aromatic part and of the aliphatic tails are nearly free whereas there is a biasing in the vicinity of the chiral centre.

The molecular tilt at the Sm A – Sm C transition induces an anisotropy in the fluctuations of the long molecular axis and a quadrupolar (bipolar) biasing of rotation around this axis. This is true for achiral as well as for chiral systems. The difference is that in chiral systems there is in addition a weak polar biasing of the rotation around this long molecular axis which is most pronounced in the vicinity of the chiral centre and nearly absent in both the aliphatic tails and the aromatic core.

ii) The dynamic properties[4] characteristic for the ferroelectric Sm C^* phase – the *amplitude* and *phase* fluctuations modes – are beginning to be observed. These properties cannot be understood within a classical model where the tilt and the polarization are strictly proportional to each other.

iii) The critical behaviour of the Sm A – Sm C^* transition can be in the experimentally accessible region described by a *mean field* Landau model with an anomalously large sixth–order term.

iv) Generalized thermodynamic models describing all these behaviour in a consistent way have been developed[5,6,7].

v) Comb–like polymeric liquid crystals exhibiting ferroelectricity have been synthesized[8].

II. SYMMETRY CONDITIONS FOR FERROELECTRICITY IN LIQUID CRYSTALS

For ferroelectricity to occur in liquid crystals the spontaneous polarization vector $\vec{P}$ has to be invariant with respect to all symmetry operations that leave the medium invariant. As liquid crystals are invariant with respect to a sign reversal of the molecular director $\vec{n}$

$$\vec{n} \rightarrow -\vec{n} \text{ (head–tail invariance)} \qquad \text{(II.1)}$$

and any component of $\vec{P}$ along $\vec{n}$ violates this condition, the polarization vector can only be non–zero if it is locally perpendicular to the molecular director:

$$\vec{P} \perp \vec{n} \qquad \text{(II.2)}$$

Nematic and Sm A type liquid crystals belong to the point group $D_{\infty h}$ if they are composed of non–chiral molecules or to the group D_{∞} if they are composed of chiral molecules. They are invariant with respect to rotations around the long molecular axis, i.e. for rotations around the director as they posses the symmetry element $C_{\infty z}$. In the Sm A phase the z axis is parallel to the normal to the smectic layers. The perpendicular component ($P_{\perp}$) of the spontaneous polarization is thus always zero and these systems cannot be ferroelectrics.

The rotational symmetry around the molecular axis ($C_{\infty z}$) vanishes in the Sm C phase where the molecules are tilted with respect to the smectic layers (Fig. 1). Here the point group symmetry is reduced for non–chiral molecules from $D_{\infty h}$ to C_{2h}. Nevertheless even here spontaneous polarization is forbidden by symmetry. This can be shown as follows[9]:

A 180° rotation around the y–axis results in:

$$\vec{P} = \begin{vmatrix} P_1 \\ P_2 \\ P_3 \end{vmatrix} \rightarrow \begin{vmatrix} -P_1 \\ P_2 \\ -P_3 \end{vmatrix} \Rightarrow P_1 = P_3 = 0 \quad . \qquad \text{(II.3)}$$

A reflection in the xz mirror plane (the plane of the tilt) results in:

$$\vec{P} = \begin{vmatrix} 0 \\ P_2 \\ 0 \end{vmatrix} \rightarrow \begin{vmatrix} 0 \\ -P_2 \\ 0 \end{vmatrix} \Rightarrow P_2 = 0 \qquad (II.4)$$

thus inducing a vanishing of ferroelectricity.

To get a non–zero spontaneous polarization the above xz reflection symmetry has to be broken. This can be done by making the molecules chiral, i.e. by introducing an asymmetric carbon or another chiral centre into the molecule. A chiral Sm C* phase may thus exhibit a non–zero spontaneous polarization perpendicular to tilt plane (Fig. 1).

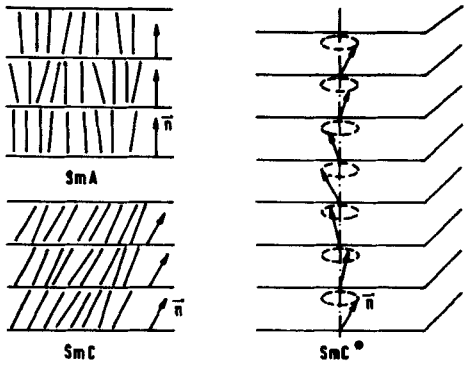

FIGURE 1. Schematic presentation of the Sm A, spatially homogeneous Sm C and spatially inhomogeneous, twisted Sm C* phase. The unit vector $\vec{n}$ points in the local preferred direction of the long molecular axes. The pitch of the helix in the Sm C* phase is much larger than the layer thickness (10^3 is a typical factor for their ratio).

Thus the spontaneous polarization will be perpendicular to the molecular director $\vec{n}$ and to the normal to the smectic planes[9,1]:

$$\vec{P}_\perp = P\vec{z} \times \vec{n} \qquad (II.5)$$

The above argument shows that $\vec{P}_\perp$ is symmetry allowed in all chiral tilted smectics of C_2 symmetry: Sm C^*, F, G, H, I, K and tilted columnar discotic phases.

It is however not symmetry allowed in cholesterics or isotropic optically active liquids. In this last case no reflections are allowed but the system has full rotational symmetry (group SO (3)).

For a 180° rotation around the y–axis one has:

$$\vec{P} = \begin{vmatrix} P_1 \\ P_2 \\ P_3 \end{vmatrix} \rightarrow \begin{vmatrix} -P_1 \\ P_2 \\ -P_3 \end{vmatrix} \Rightarrow P_1 = 0, \quad P_3 = 0 \qquad (II.6)$$

A rotation for 90° around the z–axis further results in:

$$\begin{vmatrix} 0 \\ P_2 \\ 0 \end{vmatrix} \rightarrow \begin{vmatrix} P_2 \\ 0 \\ 0 \end{vmatrix} \Rightarrow \vec{P} = 0 \qquad (II.7)$$

so that optically active isotropic media are not ferroelectric.

It should be noted that chirality in tilted smectic structures of C_2 symmetry is only a necessary and not a sufficient condition for ferroelectricity in liquid crystals. The existence of permanent electric dipole moments transverse to the long molecular axis is as well needed.

One should also note[9] that the ground state of a chiral tilted smectic in the bulk will generally not be homogeneous. It will be characterized by a spontaneous twist and a spontaneous bend: both contributions are independent and sufficient to induce a helicoidal variation of the local director.

This can be seen as follows: The nematic elastic energy density

$$g = \frac{1}{2}K_1(\text{div}\,\vec{n})^2 + \frac{1}{2}K_2(\vec{n}.\,\text{rot}\,\vec{n})^2 + \frac{1}{2}K_3(\vec{n}\times\text{rot}\vec{n})^2 \qquad (II.8)$$

– representing splay, twist and bend deformations – will be in the presence of chirality transformed to

$$(\vec{n} \cdot \text{rot}\, \vec{n})^2 \rightarrow (\vec{n} \cdot \text{rot}\, \vec{n} - q)^2 \qquad \text{(II.9a)}$$

representing a spontaneous twist characterized by q, and to

$$(\vec{n} \times \text{rot}\, \vec{n})^2 \rightarrow (\vec{n} \times \text{rot}\, \vec{n} - \vec{v})^2 \qquad \text{(II.9b)}$$

representing a spontaneous bend characterized by a vector $\vec{v} = \alpha \vec{z} \times \vec{n}$. These two contributions might even counteract each other giving a helix free tilted ferroelectric liquid crystalline state.[1]

III. TILT AND POLARIZATION IN Sm C* SYSTEMS

Ferroelectric smectic C* liquid crystals were discovered by Meyer and coworkers[1]. The smectic C phase is ferroelectric if the molecules are chiral and have a permanent dipole moment transverse to their long molecular axes. In the high temperature smectic A–phase the molecules are rotating "freely" around their long axes (Fig. 1) which are on the average oriented perpendicular to the smectic layers ($n_z = 1$, $n_x = n_y = 0$). The point symmetry of each layer corresponds to the group D_∞. The transition to the ferroelectric smectic C* phase is induced[2] by the two–dimensional representation E_1 and the point symmetry of the layers is reduced to C_2. The order parameters of the transition[2] are the molecular tilt (i.e. the quadratic combinations $\xi_1 = n_z n_x$ and $\xi_2 = n_z n_y$) and the components P_x and P_y of the in–plane spontaneous polarization (Fig. 2) which are connected with the "biasing" of the rotation of the ferroelectric dipoles around the long molecular axis. It is generally accepted that the tilt of the long molecular axes with respect to the layer normals is the primary and the spontaneous polarization the secondary order parameter. Ferroelectric liquid crystals are thus improper ferroelectrics.

The average molecular tilt as well as the in–plane spontaneous polarization slowly rotate as one goes from one smectic plane to the other resulting in a helical structure. The pitch of the helix is of the order of 10^3 interlayer distances and will be, in the general case, incommensurate with the one–dimensional translational periodicity of the smectic density modulation.

Symmetry allows[2] for two types of bilinear coupling between the molecular tilt and the spontaneous polarization: a "piezo--electric" chiral coupling

$$P_x \xi_2 - P_y \xi_1 \qquad \text{(III.1a)}$$

resulting in

$$P_x = D n_z n_y \qquad \text{(III.1b)}$$

and

$$P_y = - D n_z n_x \qquad \text{(III.1c)}$$

and a "flexo--electric" coupling[2]

$$P_x \frac{\partial \xi_1}{\partial z} + P_y \frac{\partial \xi_2}{\partial z} \qquad \text{(III.2a)}$$

resulting in a proportionality between the polarization and the bending and twisting of the molecular director in space:

$$P_x = \tilde{D} \frac{\partial \xi_1}{\partial z}, \qquad P_y = \tilde{D} \frac{\partial \xi_2}{\partial z} \quad . \qquad \text{(III.2b)}$$

Both of these couplings result in a proportionality between the tilt θ and the in--plane polarization P (Fig. 2):

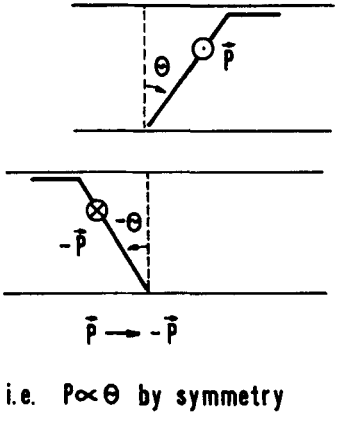

FIGURE 2:
The in--plane polarization changes its sign as the tilt angle θ is inverted in the Sm C* phase. The ice-hockey stick description of the chiral molecule illustrates the biasing of the rotation around the long molecular axis

$$P/\theta = \text{const} \neq f(T) \qquad \text{(III.3a)}$$

and

$$\theta \rightarrow -\theta\,, \quad P \rightarrow -P \quad . \qquad \text{(III.3b)}$$

Early measurements of the polarization and the tilt seemed to support this proportionality[10]. Recent almost simultaneous high resolution measurements of the polarization P and the molecular tilt angle θ in DOBAMBC have however shown[3] that the ratio P/θ remains fairly constant for $T_c - T \geqslant 2\,K$ but drops precipitously to a small but non–zero value in the region $T_c - T \leqslant 2\,K$ (Figs. 3 and 4).

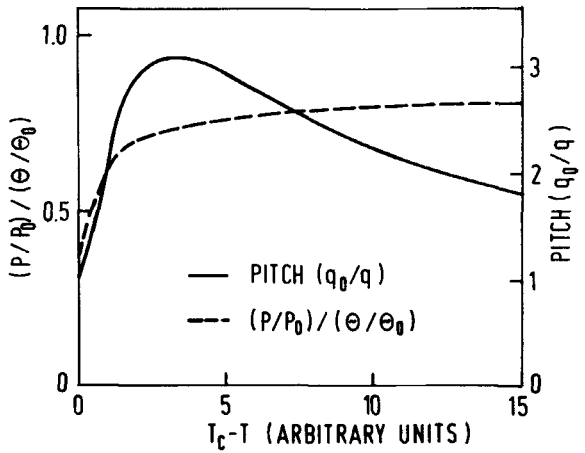

FIGURE 3. Ratio between the normalized polarization and normalized tilt versus temperature (arbitrary units). Also shown is the normalized temperature dependence of the pitch close to T_c.[3]

Measurements in other Sm C* systems have shown a similar anomaly in P/θ. Thus we see that

$$P/\theta = f(T) \qquad \text{(III.4)}$$

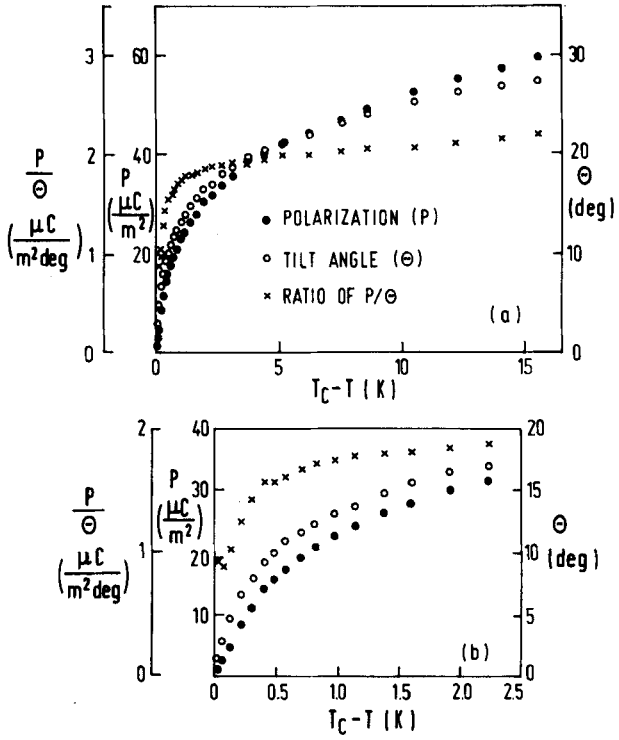

FIGURE 4. Spontaneous polarization, tilt angle, and their ratio (P/θ) vs. $T_c - T$ for DOBAMBC, (a) in a large temperature range and (b) in the vicinity of the transition.[3]

and that the simple classical mean field free energy density expression for the Sm C* phase[2,4]:

$$g(z) = \frac{1}{2}a(\xi_1^2 + \xi_2^2) + \frac{1}{4}b(\xi_1^2 + \xi_2^2)^2 - \Lambda\left(\xi_1 \frac{d\xi_2}{dz} - \xi_2 \frac{d\xi_1}{dz}\right)$$

$$+ \frac{1}{2}K_{33}\left[\left(\frac{d\xi_1}{dz}\right)^2 + \left(\frac{d\xi_2}{dz}\right)^2\right] + \frac{1}{2\epsilon}(P_x^2 + P_y^2) - \mu\left(P_x \frac{d\xi_1}{dz} + P_y \frac{d\xi_2}{dz}\right)$$

$$+ C(P_x \xi_2 - P_y \xi_1) \qquad \text{(III.5a)}$$

with

$$\xi_1 = n_z n_x = \theta \cos\phi, \; \xi_2 = n_z n_y = \theta \sin\phi, \; P_x = -P \sin\phi,$$

$$P_y = P \cos\phi \quad , \quad \phi = qz$$

or

$$g(z) = \frac{1}{2} a\theta^2 + \frac{1}{4} b\theta^4 - \Lambda\theta^2 q + \frac{1}{2} K_{33}\theta^2 q^2 + \frac{1}{2\epsilon} P^2 - \\ - \mu P\theta q + CP\theta \qquad \text{(III.5b)}$$

does not properly describe the experimental situation [3,6]. Here $a = \alpha (T - T_o)$, q is the wave vector of the Sm C* helix, K_{33} is the elastic modulus, Λ the coefficient of the Lifshitz–invariant term responsible for the helicoidal modulation and μ and C are the coefficients of the flexo–electric and piezo–electric coupling terms between the tilt angle and the polarization.

IV. CRITICAL BEHAVIOUR

Sm C* liquid crystals – similarly as Sm C and Sm A liquid crystals – belong to the d = 3, n = 2 universality class similarly as superfluids and superconductors. Here d = 3 is the number of spatial dimensions and n = 2 the number of components of the order parameter. The upper critical dimensionality above which critical fluctuations can be neglected and the mean field model is exact is $d_u = 4$. The primary order parameter for Sm C* systems is the tilt

$$\theta = |\theta| e^{i\phi} \qquad \text{(IV.1)}$$

where the phase ϕ varies in space, $\phi = \phi(z)$ whereas it is constant in Sm C systems (ϕ = const). This difference is however not relevant for the critical behaviour.

For the d = 3, n = 2 universality class renormalization group theory predicts the following values for the critical exponents β, γ, ν and α:

Tilt: $|\theta| \propto |\epsilon|^{\beta}$, $\beta = 0.35$ (IV.2a)

Susceptibility: $\chi = \chi_0 |\epsilon|^{\gamma}$, $\gamma = 1.32$ (IV.2b)

Correlation length: $\xi = \xi_0 |\epsilon|^{-\nu}$, $\nu = 0.67$ (IV.2c)

Specific heat: $C \propto |\epsilon|^{-\alpha}$, $\alpha = -0.02$ (IV.2d)

where $|\epsilon| = |(T - T_c)/T_c|$.

The temperature dependence of the tilt $|\theta|$ is consistent with the above "critical" value $\beta = 0.35$, whereas the X–ray scattering data[11] show that

$$\gamma = 0.98 \pm 0.04 \qquad \text{(IV.3)}$$

in agreement with the mean field approximation (MFA) behaviour for $\epsilon > \epsilon_c = 10^{-5}$ and definitely excluding $\gamma = 1.32$. Specific heat data[7,12] (Fig. 5) show that $\alpha = 0.5$. Scattering data[11] also show that $\nu = 1/2$ in agreement with MFA and that $\xi_0 \approx 20$ Å.

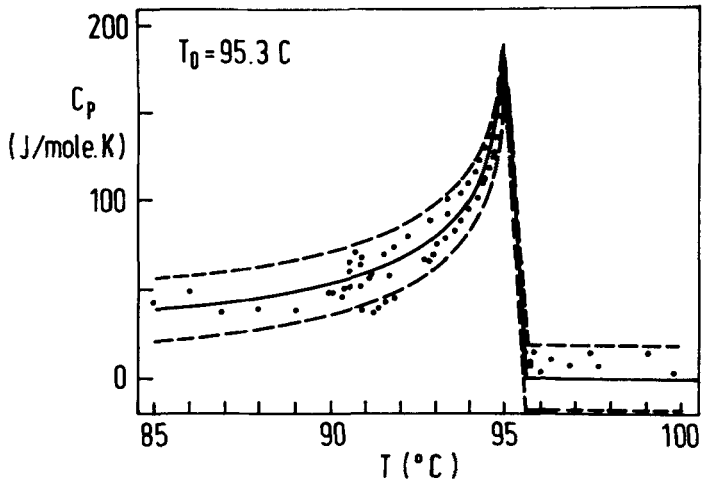

FIGURE 5: Specific heat for DOBAMBC: the dots represent measured values. The solid line represents the theoretical curve. The broken lines represent the solid line plus/minus two standard deviations of the measured values[9].

It thus seems that the true critical region is inaccessible by current experimental techniques and that the critical properties observed so far can be described by a mean field model, e.g. by a Landau theory.

The property that still has to be understood is the apparent non-classical behaviour of the tilt angle θ_o (Fig. 4) and the specific heat C_p (Fig. 5) in combination with the classical behaviour of the susceptibility and the correlation length.

Expressing the relevant part of the free energy density up to sixth order in θ as[7,12]

$$g = g_o + \frac{a}{2}\theta^2 + \frac{b}{4}\theta^4 + \frac{c}{6}\theta^6 \qquad \text{(IV.4)}$$

where $a = a'\epsilon$, b = const, c = const one finds the specific heat from

$$C_p = -T\left(\frac{d^2g}{dT^2}\right)_p \quad . \qquad \text{(IV.5)}$$

This yields in agreement with experiment

$$C_p = C_o, \quad T > T_c \qquad \text{(IV.6a)}$$

$$C_p = C_o + AT(T_o - T)^{-1/2}, \quad T < T_c \qquad \text{(IV.6b)}$$

where $T_o = T_c[1 + b^2/(4a'c)]$. The temperature dependence of the tilt angle is also modified by the presence of the large sixth order term yielding

$$\theta = \left[\frac{b}{2c}\left(-1 + \sqrt{1 + \frac{T_c - T}{\Delta T}}\right)\right]^{1/2} \quad . \qquad \text{(IV.7)}$$

This results in an apparent T—dependence of β defined as the slope of $\log\theta$ vs. $\log(T_c - T)$:

$$|\theta| \propto |\epsilon|^{1/2}, \quad |\epsilon| \ll \epsilon_o \qquad \text{(IV.8a)}$$

and

$$|\theta| \propto |\epsilon|^{1/4}, \quad |\epsilon| \gg \epsilon_o \qquad \text{(IV.8b)}$$

where $\epsilon_o = \Delta T/T_c = (b^2/4a'c\,T_c)$ and $\Delta T \approx 1$ K for DOBAMBC.

The apparent non–classical behaviour in θ is thus the result of a "tri–critical" like exponent in the MFA. The transition region from the classical value $\beta = 0.5$ to the tri–critical value $\beta = 0.25$ is broader than the experimentally useable region (Fig. 6) thus explaining the observed value of $\beta = 0.31$.

Thus classical values of the critical exponents have been observed in all quantities measured so far in Sm C* systems. The mean–field like Landau model can be thus indeed applied as critical fluctuations are negligible for $\epsilon > 10^{-5}$.

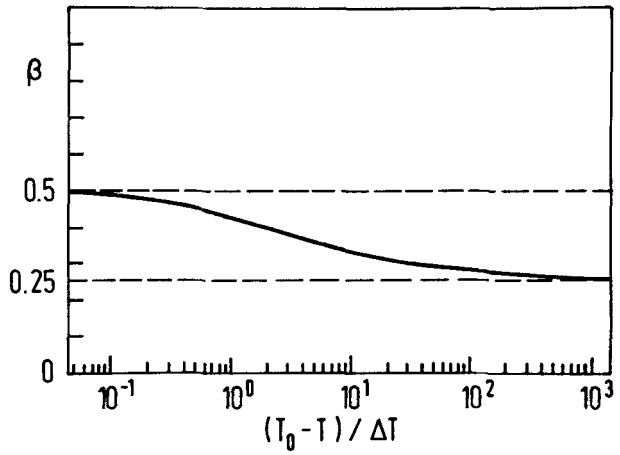

FIGURE 6. β is the slope in a log–log plot of θ vs $T_o - T$. Here β is shown as a function of temperature in a logarithmically reduced temperature scale. The transition region from the "classical" value $\beta = 0.5$ to the value 0.25 is broader than the experimentally useable region[7].

V. MICROSCOPIC DETERMINATION OF ORDER PARAMETERS WITHOUT UNWINDING THE Sm C* HELIX

All measurements of the tilt and the polarization discussed so far have been performed by methods involving the unwinding of the

Sm C* helix.

In view of the discrepancy between the predictions of the "classical" model and the experimental results, it seemed worthwhile to measure the tilt and the polarization as well as other liquid crystalline order parameters by microscopic techniques which do not require the unwinding of the helix and allow a determination of the order parameters as a function of the position of the nucleus in the molecule[13,14].

In view of that we tried to determine by nuclear magnetic resonance (NMR) and nuclear quadrupole resonance (NQR):

i) the nematic order parameter $S_{zz} = \frac{3}{2}<\cos^2\beta - \frac{1}{2}>$, where β is the deviation of the long molecular axis from its equlibrium orientation.

ii) the quadrupolar and polar biasing of the rotation of the transverse dipoles around the long molecular axis, i.e. the order parameters leading to biaxiality in the Sm C phase and to the local spontaneous polarization in the Sm C* phase

iii) the tilt of the molecules with respect to the normal to the smectic layers.

V.1. ^{14}N–Proton Nuclear Quadrupole Double Resonance

The main contribution of magnetic resonance to the physics of liquid crystals has been the determination of the local orientational order as a function of atomic position in liquid crystalline molecules.

Here we shall review[14] some recent ^{14}N nuclear quadrupole double resonance studies of orientational ordering in chiral and achiral biaxial smectics. We shall restrict ourselves to the data concerning the "body" of the molecules and shall not be concerned with the tails. The substances studied are achiral terephtal–bis–butyl–aniline (TBBA), chiral p–terephtal–bis–aminocinnamate (TBACA) and a mixture of 5 % TBACA in TBBA. In Fig. 7 we show the T–dependence of the electric quadrupole coupling constants e^2qQ/h and asymmetry parameters η of achiral TBBA and chiral TBACA together with the T–dependences of the nematic order parameter $S = \frac{1}{2}<3\cos^2\beta - 1>$ and the quadrupolar (bipolar) order parameter $<\cos 2\varphi>$ in TBBA.

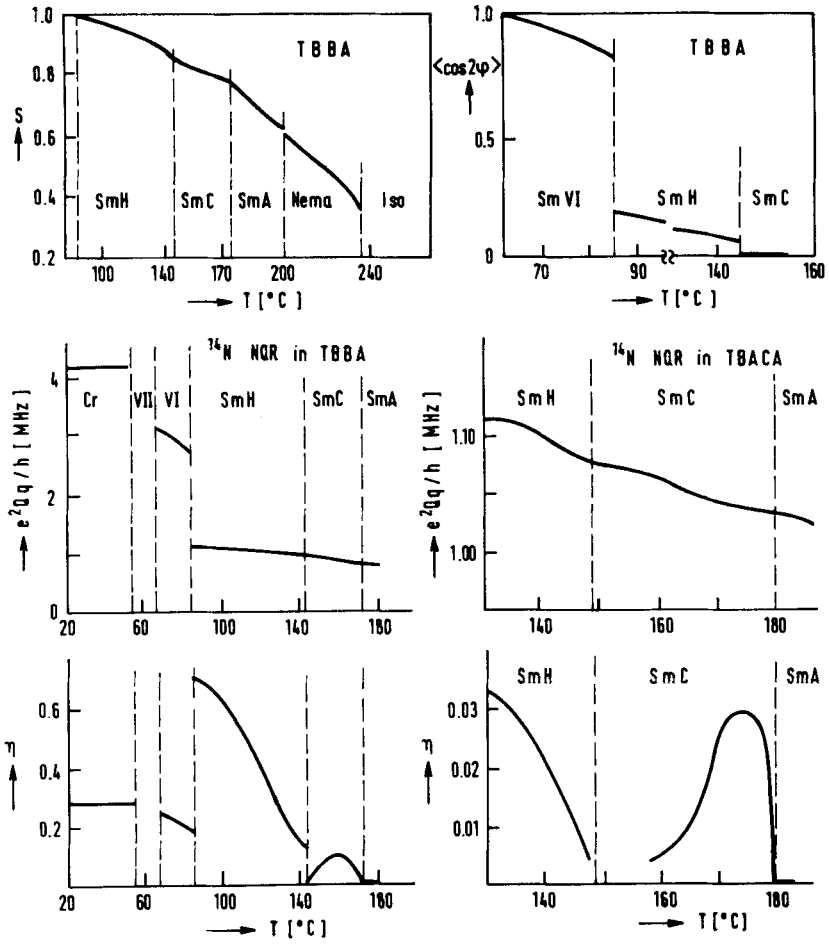

FIGURE 7. T–dependence of the nematic order parameter S in TBBA and the ^{14}N electric quadrupole coupling constant e^2Qq/h and the asymmetry parameter $\eta = V_{XX} - V_{YY}/V_{ZZ}$ in achiral TBBA and chiral TBACA. The T–dependence of the quadrupolar (i.e. bipolar) order parameter $<\cos 2\varphi>$ in TBBA is as well shown [14].

ORIENTATIONAL ORDER PARAMETER DETERMINATION VIA ^{14}N NQR: The possible biasing of the rotation of the outboard molecular dipoles (i.e. the C−N=CH−C groups) around the long molecular axis is checked via a determination of the asymmetry parameter

$$\eta = (V_{XX} - V_{YY})/V_{ZZ} \tag{V.1}$$

of the electric field gradient (EFG) tensor at the ^{14}N sites. For free uniaxial rotation, the largest principal axis V_{ZZ} will point along the long molecular axis and the EFG tensor will be axially symmetric: $V_{XX} = V_{YY}$, $\eta = 0$. Any anisotropy in the rotation around the long molecular axis will destroy the axial symmetry of the ^{14}N EFG tensor resulting in a finite η and the appearance of three ^{14}N pure NQR lines

$$\nu_{1,2} = (3/4)(eQV_{ZZ}/h)(1 \pm \eta/3) \tag{V.2}$$

$$\nu_3 = \nu_2 - \nu_1 \tag{V.3}$$

instead of a single one $\nu_1 = \nu_2$, $\nu_3 = 0$ for $\eta = 0$.

If the 5 independent EFG tensor components in the molecular frame are known and if a model for the molecular motion is assumed, one can calculate all the components of the time averaged EFG tensor and compare the resulting eQV_{ZZ}/h and η with the experiment. For uniaxial rotation we transform the EFG tensor $V_{\alpha\beta}$ from the molecular frame x_o, y_o, z_o (Table I) to a frame x, y, z rotating around the $z \parallel z_o$ axis where $x \perp y \perp z$ and $\varphi = \varphi(t)$ is the angle between x and x_o. The anisotropic fluctuations of the long molecular axis are taken into account by still another transformation to a x′, y′, z′ frame where z′ is normal to the smectic planes, x′ is the projection of the long molecular axis on the smectic plane and $y' \perp x' \perp z'$. The tilt angle $\theta(t)$ is the angle between the long molecular axis and z′, whereas $\phi = \phi(t)$ is the angle between the projections of the instantaneous and average directions of the long molecular axis on the smectic planes.

TABLE I. Rigid lattice ^{14}N quadrupole coupling tensor $V_{\alpha\beta}$ of TBBA expressed in the x_o, y_o, z_o molecular frame. Here z_o is the long molecular axis, y_o is the normal to the C−N = CH−C plane and x_o is perpendicular to y_o and z_o

$$eQV_{\alpha\beta}/h\,[MHz] = \begin{vmatrix} -3.15\ , & \pm 0.15\ , & \pm 2.41 \\ \pm 0.15\ , & 1.95\ , & \pm 0.40 \\ \pm 2.41\ , & \pm 0.40\ , & +1.20 \end{vmatrix}$$

a) **Bipolar biasing of uniaxial rotation:** For bipolar biasing of the uniaxial rotation one has $\langle\cos 2\varphi\rangle \neq 0, \langle\cos\varphi\rangle = \langle\sin\varphi\rangle = \langle\sin 2\varphi\rangle = 0$. For $\langle\cos 2\varphi\rangle \leqslant 0.3$ we now find

$$\eta = r\langle\cos 2\varphi\rangle \tag{V.4a}$$

$$eQV_{ZZ}/h = eQV_{z_oz_o}/h \tag{V.4b}$$

where $r = 2[V^2_{x_oy_o} + 1/4\,(V_{x_ox_o} - V_{y_oy_o})^2]^{1/2}/V_{z_oz_o}$.
If, on the other hand, $|r\langle\cos 2\varphi\rangle| > 1$, we get

$$\eta = |(r\langle\cos 2\varphi\rangle - 3)/(r\langle\cos 2\varphi\rangle + 1)| \tag{V.5a}$$

$$eQV_{ZZ}/h = \left|-(1/2h)\,eQV_{z_oz_o}(1 + r\langle\cos 2\varphi\rangle)\right| . \tag{V.5b}$$

b) **Polar biasing of uniaxial rotation:** For polar biasing of uniaxial rotation $\langle\cos\varphi\rangle \neq 0$, $\langle\cos 2\varphi\rangle = \langle\sin\varphi\rangle = \langle\sin 2\varphi\rangle = 0$ one gets in the limit $|\langle\cos\varphi\rangle| \ll 1$:

$$\eta = K\,.\langle\cos\varphi\rangle^2 \tag{V.6a}$$

$$eQV_{ZZ}/h = (eQV_{z_oz_o}/h)(1 + \eta) \tag{V.6b}$$

where

$$K = (2/3)\,(V^2_{x_oz_o} + V^2_{y_oz_o})/V^2_{z_oz_o}$$

c) Anisotropic fluctuations in the orientation of the axis of rotation: Anisotropic fluctuations in the direction of the long molecular axis as well result in a non–zero value of η though $<\cos 2\varphi> = <\cos\varphi> = 0$:

$$\eta = 3/2\,[<\sin\theta\cos\theta\cos\phi>^2 - <\cos^2\theta><\sin^2\theta\cos^2\phi> + \\ + <\sin^2\theta\sin^2\phi>] \qquad (V.7a)$$

$$eQV_{ZZ}/h = (eQV_{z_0z_0}/h)[1 + 3/2<\sin\theta\cos\theta\cos\phi>^2 - \\ - <\cos^2\theta><\sin^2\theta\cos^2\phi> - <\sin^2\theta\sin^2\phi>] \qquad (V.7b)$$

but the temperature dependence of η is very different from the above two cases.

Achiral TBBA: A summary of the experimental ^{14}N quadrupole coupling results is presented in Table II.

TABLE II. ^{14}N quadrupole coupling constant eQV_{ZZ}/h and asymmetry parameter η in the various phases of TBBA:

Phase	Temperature [°C]	eQV_{ZZ}/h [kHz]	η
Solid VIII	20	4220	0.260
Sm VI	70	3150	0.240
Sm H	91	1170	0.703
Sm C	150	1010	0.088
Sm A	185	810	0

A. Orientational ordering of the long molecular axis: The nematic order parameter S has been determined from the temperature dependence of the quadrupole splitting of the N = C – D deuteron line and the temperature dependence of the ^{14}N quadrupole coupling. S is zero in the isotropic phase and jumps to S = 0.32 at the isotropic–nematic transition. At the low T end of the N phase, $S \approx 0.6$. In the Sm A phase, S increases from 0.6 to 0.75 with decreasing temperature. In the Sm C it varies from 0.75 to 0.85 and in the Sm H increases from 0.85 at the high T end to 1 at the low T end of this phase.

B. Orientational ordering of the short molecular axes:

B.1. **N and Sm A phase:** Here the ^{14}N η is zero over the whole T range and $eQV_{ZZ}/h = (eQV_{z_0z_0}/h).S$. Both the fluctuations in the long molecular axis (up to 42° at the I–N transition) and the uniaxial rotation around this axis are isotropic on the NMR time scale $10^{-6} - 10^{-7}$ sec.

B.2. **Sm C phase:** The tilt in the Sm C phase induces a non–polar quadrupole–like biasing of the rotation around the long molecular axes. Here η is non–zero and exhibits a maximum in the middle of the Sm C phase, as both partial biasing of rotations around the long axis and anisotropic fluctuations of this axis with opposite T–dependences contribute to the non–zero value of η. The axial symmetry is mainly destroyed by anisotropic fluctuations in the long molecular axis, though a weak bipolar orientational ordering sets in too. We find that $\langle\cos\varphi\rangle = \langle\sin\varphi\rangle = \langle\sin 2\varphi\rangle = 0$ but $\langle\cos 2\varphi\rangle \neq 0$. The value of the bipolar order parameter is only $\langle\cos 2\varphi\rangle \approx 5 \times 10^{-3}$. The fluctuations in the tilt angle remain practically constant ($\langle\delta\theta^2\rangle^{1/2} \sim 22°$), but the azimuthal fluctuations $\langle\phi^2\rangle^{1/2}$ increase with increasing temperature resulting in a vanishing of bias at T_c.

B.3. **Sm H phase:** The occurrence of a huge temperature variation in η and the small temperature variation in e^2Q/h demonstrate the occurrence of significant bipolar orientational ordering. Expression (4a) with $r = 4.49$ well represents the experimental data. $\langle\cos 2\varphi\rangle$ varies from 0.07 at the high T end to 0.16 at the low T end of the Sm H phase.

The physical model for the molecular motion is as follows: The rigid "body" of the TBBA molecule is reorienting in a six–well potential around the long molecular axis. Four equlibrium sites are equivalent and have an occupation probability p_2 while the other two – separated by 180° – have a lower energy and an occupation probability $p_1 > p_2$. The bipolar order parameter is now given by

$$\langle\cos 2\varphi\rangle = 2(p_1 - p_2) \qquad \text{(V.8a)}$$

with

$$2p_1 + 4p_2 = 1 \qquad \text{(V.8b)}$$

whereas

$$\langle \cos\varphi \rangle = \langle \sin\varphi \rangle = \langle \sin 2\varphi \rangle = 0 \quad . \qquad \text{(V.8c)}$$

At the low T end of the Sm H phase we find from $\langle \cos 2\varphi \rangle = 0.15$ the occupation probabilities $p_2 = 0.14$ and $p_1 = 0.22$.

B.4. **Sm VI phase:** The T–dependence of the ^{14}N eQV_{ZZ}/h and η in the Sm VI phase can be described by expressions (5a) and (5b) with $eQV_{z_0z_0}/h = 1.18$ MHz and $r = 4.49$. On going from the Sm H to the Sm VI phase $\langle \cos 2\varphi \rangle$ jumps from 0.17 to about 0.85 resulting in a change in the direction of the largest principal axis of the ^{14}N EFG tensor. With decreasing T $\langle \cos 2\varphi \rangle$ increases from 0.85 at 82.5°C to 1 at 70°C.

The four high energy states in the six–well potential are now nearly empty as $p_2 = 0.02$ at 85°C and $p_2 = 7 \times 10^{-3}$ at 72°C whereas p_1 approaches 0.5. The molecular motion at the low T end of the Sm VI phase can be thus indeed described as 180° orientational jumps of the central part of the TBBA molecule, where $\langle \cos 2\varphi \rangle = 1$, $\langle \sin\varphi \rangle = \langle \sin 2\varphi \rangle = \langle \cos\varphi \rangle = 0$.

B.5. **Crystalline VIII phase:** On going from the Sm VI to the Sm VIII phase, the 180° jumps freeze out so that $\langle \cos 2\varphi \rangle = \langle \cos\varphi \rangle = 1$, $\langle \sin\varphi \rangle = \langle \sin 2\varphi \rangle = 0$, and the rigid lattice ^{14}N EFG tensor given in Table I is obtained. The freeze out probably happens in the Sm VII phase. In the crystalline VIII phase, on the other hand, the C–N = CH–C groups are already completely rigid as neither eQV_{ZZ}/h nor η vary with temperature.

V.2. ^{13}C NMR–Chemical Shift Spectroscopy[13] of DOBAMBC and HOBACPC

The temperature dependences of the ^{13}C chemical shifts of DOBAMBC and HOBACPC in the isotropic, smectic A and smectic C* phases are presented in Figures 8 and 9 together with the assignation of the 22

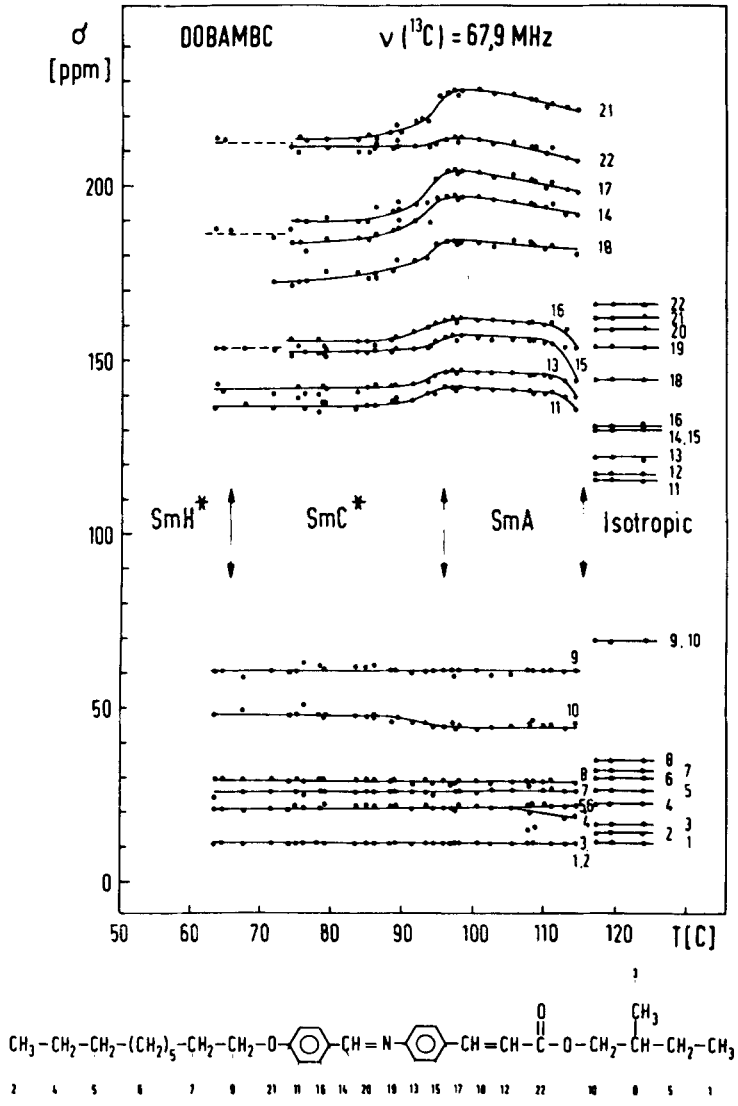

FIGURE 8. Temperature dependence of ^{13}C chemical shifts of DOBAMBC with respect to TMS in the isotropic, Sm A and Sm C* phases. The numbering of the carbons is as well shown[13].

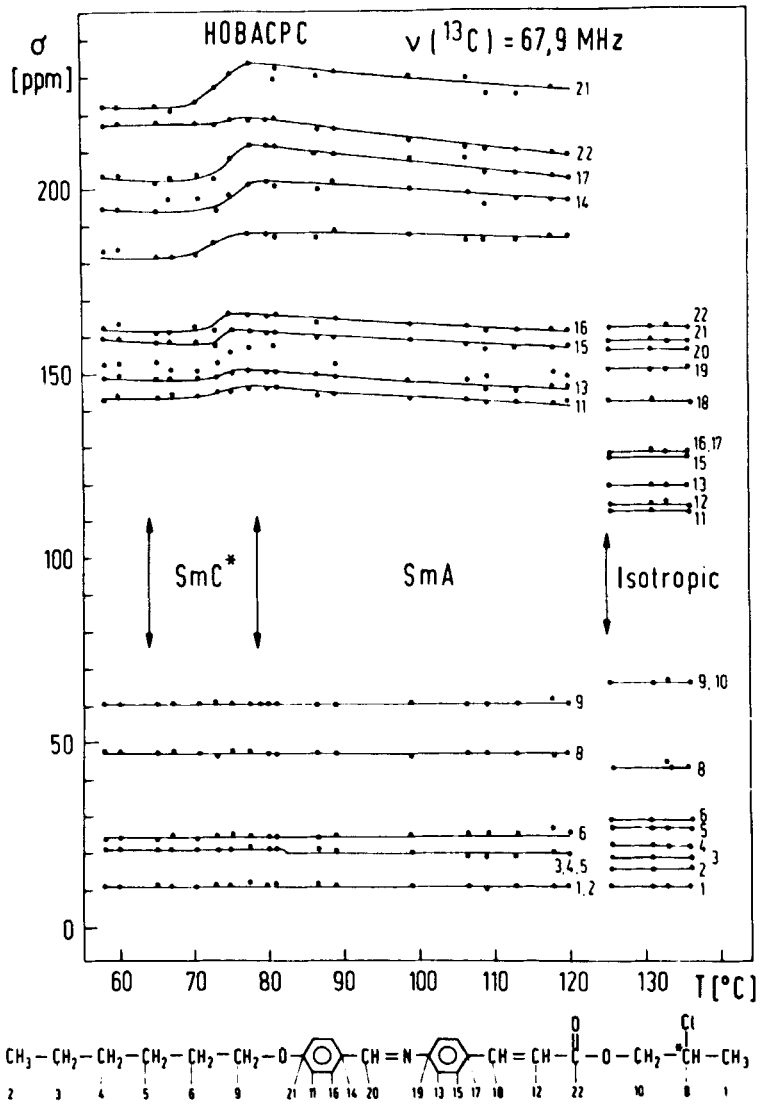

FIGURE 9: Temperature dependence of the ^{13}C chemical shifts of HOBACPC with respect to TMS in the isotropic, Sm A and Sm C* phases. The numbering of the carbons is as well shown[13].

resolved chemically non–equivalent ^{13}C lines. The assignation was performed with the help of selective proton decoupling and proton T_1 measurements as well as by comparison with the chemical shifts in other nematic and smectic liquid crystals.

The ^{13}C line of the terminal $-CH_3$ group appears at the high field part of the spectrum. It has the largest screening and therefore the smallest chemical shift with respect to TMS. The aliphatic ^{13}C resonances of both DOBAMBC and HOBACPC show up at higher magnetic fields (i.e. lower chemical shifts with respect to TMS) than the aromatic ^{13}C resonances. The C(8)–Cl NMR line in HOBACPC could not be observed.

On going from the isotropic to the Sm A phase one observes a large abrupt change in the ^{13}C chemical shifts. There is a downfield shift of the aromatic and an upfield shift of the aliphatic lines.

On going from the Sm A into the Sm C* phase there is a pronounced continuous upfield shift of the aromatic carbon lines as well as of the line of the C=O group in both DOBAMBC and HOBACPC. The change in the position of the aliphatic lines is relatively small.

i) Isotropic Phase: In view of the fast random rotational and translational molecular motion one observes in the isotropic phase only the isotropic part of the ^{13}C chemical shift tensor σ:

$$\sigma_i = \frac{1}{3} \mathrm{Tr}\, \sigma \qquad (V.9)$$

whereas the anisotropic part is averaged out to zero.

ii) Sm A Phase: When the sample is slowly cooled from the isotropic into the Sm A phase the molecules order in such a way that the normals to the smectic layers are parallel to the direction of the external magnetic field $\vec{H}$. The chemical shift tensor is not anymore isotropic. The relevant molecular motions, which are averaging the ^{13}C chemical shift tensor, are:

– fast molecular rotations around the long molecular axis, and
– fluctuations of the long molecular axis around the molecular director $\vec{n}$ which is parallel to $\vec{H}$ and thus also to the normals to the smectic layers.

The component of the chemical shift tensor in the direction of the external magnetic field $\sigma = <\sigma_{z'z'}> \equiv <\sigma_H>$ is obtained as:

$$\sigma = \sigma_i + \frac{2}{3}[\sigma_{zz} - \frac{1}{2}(\sigma_{xx} + \sigma_{yy})]S_{zz} + \frac{1}{3}(\sigma_{xx} - \sigma_{yy})(S_{xx} - S_{yy}) \tag{V.10}$$

where

$$S_{zz} = S = <\frac{3}{2}\cos^2\beta - \frac{1}{2}> \tag{V.11a}$$

measures the amount of "nematic" ordering of the long molecular axis around the molecular director $\vec{n}$, and

$$S_{xx} - S_{yy} = \frac{3}{2}<\sin^2\beta\cos 2\phi) \tag{V.11b}$$

measures the asymmetry in the fluctuations of the long molecular axis around the x and y axis. The time independent coordinate frame x', y', z' and the molecular fixed frame x, y, z are illustrated in Figure 10. The z' axis is parallel to the normal to the smectic layers whereas the x' axis points along the direction of the projection of the long molecular axis on the smectic layer. The angle $\beta(t)$ measures the fluctuations of the long molecular axis in the polar and the angle $\phi(t)$ in the azimuthal direction. The angle $\varphi(t)$ measures the orientation of the short molecular axis as the molecule rotates around its long axis. $\sigma_{xx} - \sigma_{yy}$ is of the order of 100 ppm for the aromatic carbons. Fast conformational changes – like 90° flips of benzene rings around the para-axis – effectively average out this difference so that

$$\sigma_{xx} = \sigma_{yy} \ . \tag{V.11c}$$

Expression (V.10) thus simplifies to

$$\sigma = \sigma_i + \frac{2}{3}S(\sigma_{\parallel} - \sigma_{\perp}) \tag{V.11d}$$

where $\sigma_{\parallel} = \sigma_{zz}$ is the component along the direction of the long molecular axis and $\sigma_{\perp} = \frac{1}{2}(\sigma_{xx} + \sigma_{yy})$ is the average component in the x–y plane.

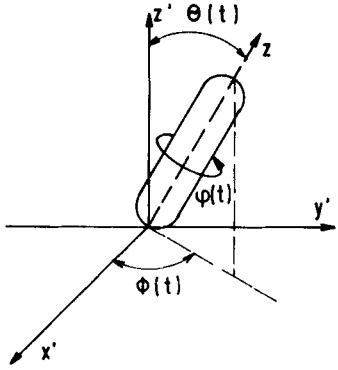

FIGURE 10. Relation between the molecular frame x, y, z and the time independent frame x', y', z'$\|H_0$

Since for the aromatic ^{13}C nuclei the heaviest shielding[15] occurs perpendicular to the aromatic plane whereas for the aliphatic groups the most shielded element of σ lies parallel to the chain axis we expect at the isotropic – Sm A transition a downfield shift of the aromatic ($\sigma_\parallel - \sigma_\perp > 0$) and an upfield shift ($\sigma_\parallel - \sigma_\perp < 0$) of the aliphatic lines. This is exactly what has been indeed observed.

The S–value for the C=O group which is the main ferroelectric dipole in the structure can also be obtained from the ^{13}C data. The directions of the principal axes of the σ tensor for this group are illustrated in Figure 11. σ_{33} = 167 ppm is here perpendicular to the COO^- plane whereas σ_{22} = 207 ppm is nearly parallel to the C=O bond direction. σ_{11} equals 317 ppm [15] and is approximately parallel to the long molecular axis. One thus finds that $\Delta\sigma$ = 130 ppm and the S values in both DOBAMBC and HOBACPC vary from S = 0.55 at the Sm A isotropic transition to S = 0.6 at the Sm A – Sm C* transition.

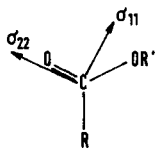

FIGURE 11. The directions of the principal axes of the chemical shift tensor of the carbonyl carbons. σ_{33} is here perpendicular to the molecular group plane.

The observation that the C=O S-values are significantly smaller than for the aromatic carbons agrees with the fact that the ordering of the aliphatic tail is always smaller than the ordering of the central aromatic part.

iii) Sm C* Phase: On going from the Sm A to the Sm C* phase a steady increase in S and a corresponding increase in the aromatic ^{13}C chemical shifts is expected. This effect is indeed seen in achiral HOAB [14] but not in chiral DOBAMBC and HOBACPC where a significant decrease of the ring and C=O ^{13}C chemical shifts is observed. This effect can be understood if one assumes that in chiral systems the helicoidal axis and the normals to the smectic layers remain parallel to the direction of the external magnetic field, whereas the long molecular axes are tilted with respect to the field direction. This is opposite to the behaviour of achiral Sm C systems where the long molecular axes are oriented parallel to the field whereas the layer normals are tilted.

If the onset of the molecular tilt with respect to the magnetic field direction would be the only change which takes place at the Sm A – Sm C* transition, the observed chemical shifts in the Sm C* phase would be given by:

$$\sigma = \sigma_i + \frac{2}{3} S (\sigma_\parallel - \sigma_\perp)\left(\frac{3}{2}\cos^2\theta_o - \frac{1}{2}\right). \qquad (V.12)$$

Here θ_o is the average molecular tilt angle and the fluctuations in the direction of the long molecular axis are assumed to be isotropic. This expression thus allows for a microscopic determination of the tilt angle without unwinding the helix.

Eq. (V.12) predicts that in the Sm C* phase the temperature dependence of

$$\frac{\sigma - \sigma_i}{\frac{3}{2}\cos^2\theta_o - \frac{1}{2}} = \frac{2}{3}(\sigma_\parallel - \sigma_\perp)S \qquad (V.13)$$

should reflect the temperature dependence of S which is known to increase monotonically with decreasing temperature. Since the T–dependence of the molecular tilt angle is known from independent optical measurements for both DOBAMBC and HOBACPC the above

prediction can be easily checked.

Figure 12 a,b,c shows the T–dependence of $\sigma - \sigma_i$ near the Sm A – Sm C* transition for the aromatic carbon in the para-position ^{13}C (17), the carbonyl carbon ^{13}C (22) in DOBAMBC and the aliphatic carbon ^{13}C (18). In all above figures the experimental data $(\sigma - \sigma_i)$ are designated by circles whereas the crosses show the calculated T–dependence of $(\sigma - \sigma_i)/(\frac{3}{2}\cos^2\theta_o - \frac{1}{2})$. The dotted line shows the T–dependence of $\frac{2}{3}S(\sigma_\parallel - \sigma_\perp)$ obtained by linear extrapolation of S from the Sm A into the Sm C* phase. If Eq. (V.13) is correct, the crosses and the dotted lines should lie on top of each other.

The above comparison demonstrates that Eq. (V.13) adequately describes the experimental situation for most aliphatic carbons. It can be used to determine the T–dependence of the tilt angle. For HOBACPC we find $\theta_o = k(T_c - T)^{0.35\pm0.05}$ with $k = 0.18\,[K^{0.35}]^{-1}$ in relatively good agreement with the optical tilt angle measurements involving the unwinding of the helix. A similar relation $\theta_o = k(T_c - T)^{0.30\pm0.05}$ with $k = 0.21\,[K^{0.3}]^{-1}$ holds for DOBAMBC and is in excellent agreement with the optical measurements (Fig. 13).

There are however deviations from this relation for the aromatic carbons and for the C=O group in both DOBAMBC and HOBACPC.

This discrepancy can be the result of:

i) an anisotropy in the fluctuations of the long molecular axis around $\vec{n}$.

ii) a polar biasing of the molecular rotation around the long molecular axis, or

iii) a bipolar biasing of the molecular rotation around the long molecular axis.

All of these effects can of course also occur simultaneously. In such a case Eq. (V.13) has to be extended to

$$\frac{\sigma - \sigma_i}{\frac{3}{2}\cos^2\theta_o - \frac{1}{2}} = \frac{2}{3}(\sigma_\parallel - \sigma_\perp)S + \Delta(T) \qquad \text{(V.14a)}$$

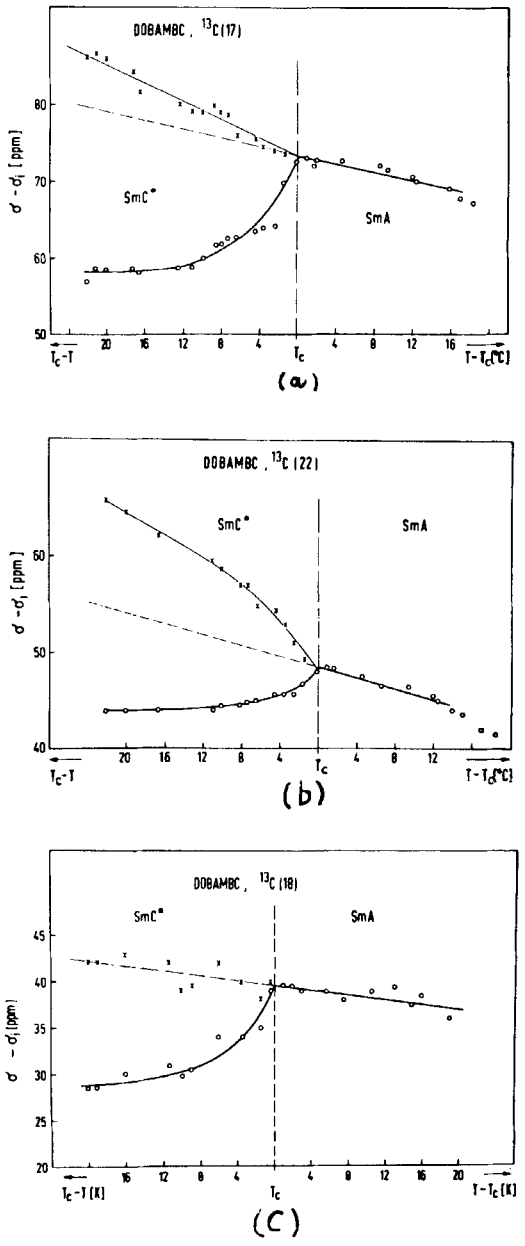

FIGURE 12. Temperature dependence of $\sigma - \sigma_i$ (circles) near the Sm A – Sm C* transition in DOBAMBC for (a) the aromatic carbon in the para–position C (17). (b) the carbonyl carbon C (22), (c) the aliphatic carbon C (18). The crosses show the calculated T–dependence of $(\sigma - \sigma_i)/(\frac{3}{2}\cos^2\theta_o - \frac{1}{2})$ whereas the dotted line shows the T–dependence of $\frac{2}{3}S(\sigma_\parallel - \sigma_\perp)$ obtained by a linear extrapolation of S from the Sm A into the Sm C* phase. The experimental data are designated by circles

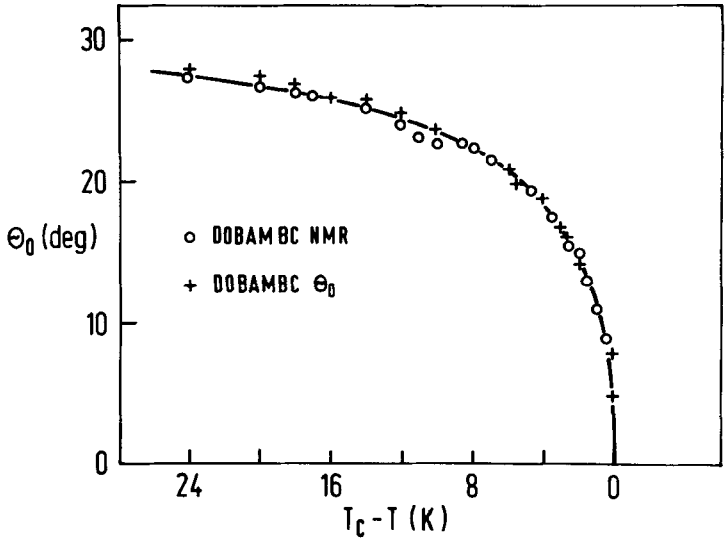

FIGURE 13. Temperature dependence of the molecular tilt angle θ_o in DOBAMBC as derived from ^{13}C NMR of aliphatic carbons. The optical data are shown for comparison[10].

where

$$\Delta = \Delta_a + \Delta_p + \Delta_{bp} \quad . \tag{V.14b}$$

with Δ_a, Δ_p and Δ_{bp} standing for the contributions due to anisotropic fluctuations, polar and bipolar biasing respectively. For DOBAMBC at $T = T_c - 20$ K, $\Delta \cong 10$ ppm for the C=O group, 3 ppm for the aromatic carbons at the ortho– and $\Delta = 1.5$ ppm for the aromatic carbons at the para-sites. For HOBACPC $\Delta = 9$ ppm for the C = O group at $T = T_c - 10$ K.

If the deviations from Eq. (V.13) are due to the anisotropy in the fluctuations around the molecular director $\vec{n}$, $\Delta(T)$ is given by:

$$\Delta_a(T) = (\sigma_\parallel - \sigma_\perp) \frac{\sin^2 \theta_o}{3\cos^2 \theta_o - 1} < \sin^2 \beta \cos 2\phi > \tag{V.15a}$$

whereas

$$\Delta_p(T) = 4\sigma_{xz}\frac{\sin 2\theta_o}{3\cos^2\theta_o - 1}\langle\cos\varphi\rangle \qquad \text{(V.15b)}$$

if the observed deviation is the result of a polar biasing of the molecular rotation around the long molecular axis.

If the observed deviation is due to a "bipolar" biasing of the molecular rotation we get

$$\Delta(T)_{bp} = 2(\sigma_{xx} - \sigma_{yy})\frac{\sin^2\theta_o}{3\cos^2\theta_o - 1}\langle\cos 2\varphi\rangle \qquad \text{(V.15c)}$$

Let us now analyze each of these contributions separately.

We shall first treat the case when the rotation around the long molecular axis is free, i.e. $\langle\cos\varphi\rangle = 0$, $\langle\cos 2\varphi\rangle = 0$ and $\Delta \cong \Delta_a$ is due to anisotropic fluctuations of the long molecular axis around $\vec{n}$. For DOBAMBC at $T = T_i - 20$ K one finds from the experimental data for the C=O group within this model

$$\frac{\langle\sin^2\beta\cos 2\phi\rangle}{S} = 0.73 \qquad \text{(V.16a)}$$

For strongly anisotropic fluctuations, where $\cos 2\phi = 1$, we have

$$\langle\sin^2\beta\cos 2\phi\rangle_{max} = \langle\sin^2\beta\rangle = \frac{2}{3}(1 - S)\,. \qquad \text{(V.16b)}$$

This yields $\langle\sin^2\beta\cos 2\phi\rangle_{max} = 0.35$ and $S = 0.48$. The value of S derived from this model is much too small as S for the C=O group equals ~ 0.6 even in the Sm A phase. Anisotropic fluctuations are thus not capable of explaining the observed value of Δ for the C=O group though they yield a large enough effect to be capable of explaining the observed Δ–values for the aromatic carbons in agreement with the ^{14}N data in TBBA. The same conclusion is true for HOBACPC.

The observed values of $\Delta(T)$ can be however satisfactorily explained by polar biasing of the molecular rotation around the long molecular axis. For the C=O group one can get from the literature[15] the off–diagonal component σ_{xz} as $\sigma_{xz} = 80$ ppm. Evaluating the numerical values of the prefactors in the expressions (15b) and (15c)

one finds for the polar term $\Delta_p \cong 320 <\cos\varphi>\theta_o$ ppm whereas $\Delta_{bp} \cong 40 <\cos 2\varphi>\theta_o^2$ ppm, so that $\Delta_{bp} \ll \Delta_p$, though $<\cos\varphi>$ and $<\cos 2\varphi>$ would be comparable. Expression (15b) now yields for $\Delta \cong \Delta_p$ for DOBAMBC at $T = T_c - 20$ K as an upper limit for the polar ordering:

$$<\cos\varphi> \cong 5 \times 10^{-2} \qquad \text{(V.17a)}$$

whereas

$$<\cos\varphi> \cong 7 \times 10^{-2} \qquad \text{(V.17b)}$$

for HOBACPC at the low temperature edge of the Sm C^* phase, i.e. at $T = T_c - 10$ K.

The above "microscopic" values of $<\cos\varphi>$ are somewhat higher than those obtained from macroscopic measurements[3] of the spontaneous polarization where the pitch is unwound. For DOBAMBC at $T = T_c - 20$ K one finds from macroscopic measurements $<\cos\varphi> = 4 \times 10^{-2}$ whereas one gets for HOBACPC $<\cos\varphi> = 1.3 \times 10^{-2}$. The order of magnitude of $<\cos\varphi>$ is however the same in both cases.

For the aromatic carbons in the para-positions $\sigma_{xz} \cong 0$. For the ortho–carbons $\sigma_{xz} \cong 100$ ppm. From the measured Δ value of 2 ppm for the ortho–carbons one thus finds for the aromatic rings in DOBAMBC as an upper limit

$$<\cos\varphi> \cong 8 \times 10^{-3} \ . \qquad \text{(V.17c)}$$

This demonstrates that the rotation of the central part of the DOBAMBC molecule in the Sm C^* phase is nearly free. The above conclusion agrees with the ^{14}N quadrupole coupling measurements of $<\cos\varphi>$ in the Sm C^* phase of chiral TBACA.

The molecular rotation is however biased in the neighbourhood of the chiral centre and the polar C=O group which is the main ferroelectric dipole in the structure. This is clearly demonstrated in the case of C(10) carbon in DOBAMBC where–in contrast to other aliphatic carbons–Δ is rather large and clearly results from polar

ordering, $<\cos\varphi> \neq 0$.

The temperature dependence of the "biasing" shift for the C=O group in DOBAMBC and HOBACPC close to the Sm A – Sm C* transition provides an additional argument for the validity of the approximation $\Delta \cong \Delta_p$ (Fig. 14). Over most of this temperature range $\Delta \propto (T_c - T)^{0.7}$ for both DOBAMBC and HOBACPC. This agrees with the expected temperature dependence of the polar "biasing" shift

$$\Delta_p \propto \theta_o <\cos\varphi> \tag{V.18}$$

as both θ_o and $<\cos\varphi>$ should be proportional to $(T_c - T)^{\beta}$ with $\beta \cong 0.35$. It does not agree with the expected temperature dependence of the bipolar shift

$$\Delta_{bp} \propto \theta_o^2 <\cos 2\varphi> \tag{V.19}$$

Similar results have been obtained for MORA–8, DOBA–1–MPC and other ferroelectric liquid crystals. In all these systems the order parameters have been determined as a function of the position of the nucleus in the molecule.

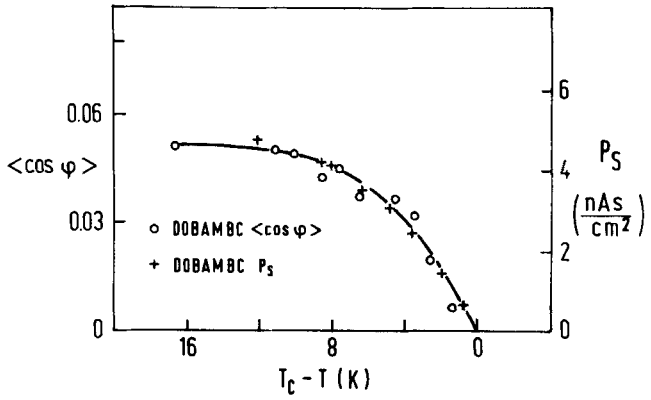

FIGURE 14. Temperature dependence of the polar order parameter $<\cos\varphi>$ of the C=O group in DOBAMBC. The T–dependence of the macroscopic spontaneous polarization is shown for comparison [10].

It should be stressed that the above microscopic determination of the order parameters agrees rather well with the more conventional macroscopic one. This is also true for the recent measurement of the molecular tilt via a simultaneous determination of the optical rotatory power and the T–dependence of the pitch of the helix in DOBAMBC[16].

VI. DYNAMICAL PROPERTIES

Ferroelectric Sm C* type liquid crystals represent an incommensurate spatially modulated structure. The tilt of the long molecular axis from the normal to the smectic layers precesses helicoidally as one goes from one smectic layer to another. The periodicity of the helicoidal modulation (a_2) is incommensurate to the periodicity of the spacing between the smectic layers (a_1):

$$\frac{a_2}{a_1} \neq \frac{M}{N} ; \quad M, N = 1, 2, 3 \ldots . \tag{VI.1}$$

The primary order parameter is two–dimensional [2,4]

$$\xi_1 = n_x n_z , \quad \xi_2 = n_y n_z \tag{VI.2}$$

and can be, for small tilt angles, expressed as:

$$\xi_1 = \theta_o \cos(qz) , \qquad \xi_2 = \theta_o \sin(qz) \tag{VI.3}$$

where θ_o is the magnitude of the tilt angle and q the wave vector of the helix ($q = 2\pi/a_2$). A characteristic property of such incommensurate systems is that the soft mode of the high temperature (Sm A) phase splits at T_c into two modes: an *amplitude fluctuation mode* (amplitudon), involving a change in the magnitude of the order parameter (i.e. a change in the magnitude of the tilt angle θ_o), and a *phase fluctuation mode* (phason) involving a change in the position of the modulation wave (i.e. a sliding of the chiral helix through the system).

The amplitudon is just a soft optic mode. The phason on the other hand, is acoustic–like and represents the Goldstone mode recovering the symmetry lost at the Sm A – Sm C* transition. For the critical wave vector k = q it thus represents a "gapless" excitation $\omega_{\text{phason},k=q} = 0$.

The dynamical properties of the Sm A – Sm C* transition have been studied by Blinc and Žekš[4] as early as 1978! Generally we have:

$$\omega^2_{\text{amplitudon}} = 2A(T_c - T) + \kappa^2 (k - q)^2 \qquad \text{(VI.4a)}$$

$$\omega^2_{\text{phason}} = \kappa^2 (k - q)^2 \qquad \text{(VI.4b)}$$

In crystalline incommensurate systems the phason is generally pinned by impurities or discrete lattice effects so that this excitation is not truly gapless:

$$\omega^2_{\text{phason}} = \kappa^2 (k - q)^2 + \Delta^2_{\text{impurities}} \qquad \text{(VI.5)}$$

The phason gap $\Delta_{\text{impurities}}$ is in solids of the order of $10^{10} - 10^{11}$ Hz. In liquid crystalline systems pinning is absent and the phason mode should be truly gapless.

It has been studied by dielectric spectroscopy[17] and laser optical mixing spectroscopy[18].

Dielectric spectroscopy of the Sm A – Sm C* transition is based on the fact that – because of the chirality of the molecules – the tilt locally breaks the axial symmetry around the long molecular axis and induces a transverse in–plane polarization:

$$P_x = -P_0 \sin(qz) \qquad P_y = P_0 \cos(qz) \qquad \text{(VI.6)}$$

An electric field applied parallel to the layers will change both the magnitude and the phase of the tilt and the polarization

$$\delta\xi_1 = \delta\theta_1 \cos(qz) - \delta\theta_2 \sin(qz) \qquad \text{(VI.7a)}$$

$$\delta\xi_2 = \delta\theta_1 \sin(qz) + \delta\theta_2 \cos(qz) \qquad \text{(VI.7b)}$$

$$\delta P_x = -\delta P_1 \sin(qz) - \delta P_2 \cos(qz) \qquad \text{(VI.7c)}$$

$$\delta P_y = +\delta P_1 \cos(qz) - \delta P_2 \sin(qz) \qquad \text{(VI.7d)}$$

thus separating the dielectric response

$$\chi = \lim_{E \to 0} \langle P_i \rangle / E \qquad \text{(VI.8a)}$$

into two modes:

$$\langle P_i \rangle = \langle P_{i1} \rangle + \langle P_{i2} \rangle \qquad \text{(VI.8b)}$$

$$\chi = \chi_1 + \chi_2 \qquad \text{(VI.8c)}$$

corresponding to amplitudon (χ_1) and phason (χ_2) contributions. From the classical Landau model of the Sm A – Sm C* transition one finds for the Sm C* phase

$$\chi = \chi_1 + \chi_2 = \frac{1}{2} \epsilon^2 C^2 \left[\frac{1}{2A(T_c - T) + K_{33} q^2} + \frac{1}{K_{33} q^2}\right] + \epsilon \,, \quad T < T_c \qquad \text{(VI.9a)}$$

and for the Sm A phase:

$$\chi = \frac{\epsilon^2 C^2}{A(T - T_c) + K_{33} q^2} + \epsilon \,, \qquad T > T_c \,. \qquad \text{(VI.9b)}$$

The phason mode contribution is here proportional to the square of the helical pitch and should be nearly T–independent close to T_c whereas the amplitudon contribution should give rise to a peak at T_c. Experimentally a peak in χ is observed *below* and not at T_c. If however the phason contribution is suppresed by a strong enough d.c. electric field (which unwinds the helix) a small peak is indeed observed at T_c as expected for the amplitudon contribution.

The temperature dependences of the soft mode, the amplitudon and the phason contributions to the static dielectric constant $\epsilon - \epsilon_\infty$ are shown in Fig. 15 a–b. The phason contribution is in the Sm C* phase for about two orders of magnitude stronger than the amplitudon

one and shows a peak 2 to 3 K below T_c. The T–dependence of this contribution does not coincide with the T–dependence of the pitch. The amplitudon contribution shows a peak at T_c.

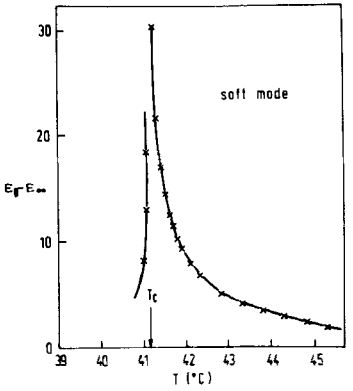

FIGURE 15a. T–dependence of the dielectric strength of the soft mode ($T > T_c$) and the amplitudon mode ($T < T_c$) for ferroelectric liquid crystal Mi–2.

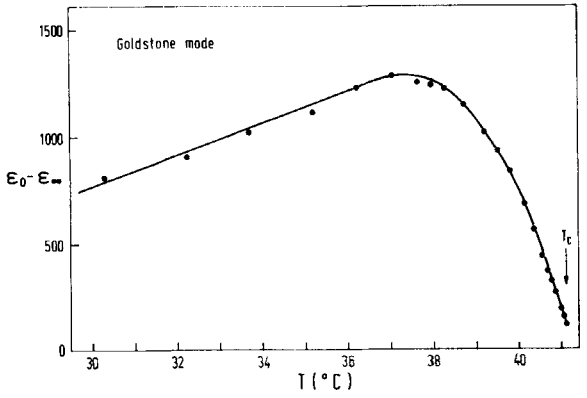

FIGURE 15b. T–dependence of the dielectric strength of the phason mode in the Sm C* phase for Mi–2.

Fig. 16 shows the frequencies (inverse relaxation times) of the soft mode, the amplitudon and the phason (Goldstone mode) excitations in the ferroelectric liquid crystal Mi–2 as functions of temperature. The frequency of the soft mode in the Sm A phase lies in the 40 – 1 kHz range in the interval $4\ K \leqslant T - T_c \leqslant 0\ K$ and sharply increases with decreasing temperature below T_c. The phason (Goldstone mode) frequency is nearly T independent. It is extremely low and lies below 50 Hz as expected for a gapless excitation. It should be noted that for dielectric spectroscopy $k \cong 0$ so that $\omega_{phason} = \kappa q$ and not strictly zero as for $k = q$. The above observation thus represents the lowest phason mode observed so far. The corresponding dispersion relations were determined by light mixing spectroscopy[18].

The discrepancy between the predicted (T–independent) and observed contribution of the phason mode to the static dielectric constant (which exhibits a peak below T_c) can be removed by extending the classical free energy density to include non–chiral terms[5] of the form $(P_x \xi_2 - P_y \xi_1)^2$ which destroy the strict proportionality between the polarization and the tilt. In this case one finds

$$\chi_2 = \frac{1}{8\pi^2 K_{33}} \left[\frac{P_o p}{\theta_o}\right]^2 \qquad \text{(VI.10)}$$

in good agreement with experiment.

Here K_{33} is an elastic constant and $p = 2\pi/q$ is the pitch of the helix. If $P_o \propto \theta_o$, the above expression reduces to χ_2 as given by (VI.9a).

Recent light scattering results on DOBAMBC have – with the help of optical mixing spectroscopy – confirmed the dielectric results and directly demonstrated both the critical slowing down of the soft mode above T_c as well as the splitting of this mode into a relatively fast (10 kHz) amplitudon mode and a slow (~ 100 Hz) phason mode.

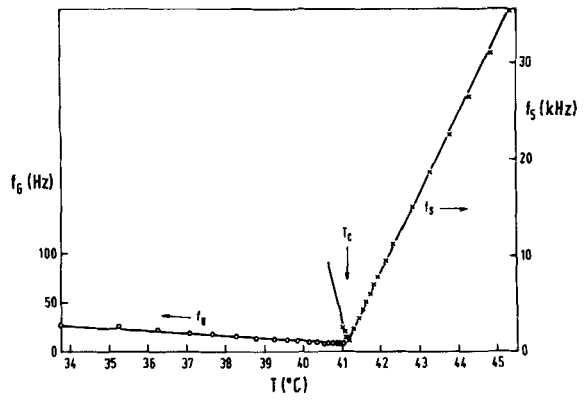

FIGURE 16. T–dependence of the frequencies of the soft mode ($T > T_c$) as well as the amplitudon and the phason mode ($T < T_c$) for ferroelectric liquid crystals Mi–2.

VII. PHASE DIAGRAM IN EXTERNAL MAGNETIC[19] AND ELECTRIC[20] FIELDS

a) **In the presence of a magnetic field** H[19] applied in a direction perpendicular to the helical axis, a term

$$\Delta g_H = -\frac{1}{2}\chi_a H^2 n_x^2 n_z^2 \qquad \text{(VII.1)}$$

has to be added to the free energy density (III. 5 a). The magnetic field tends to align the molecules because of their magnetic anisotropy $\chi_a = \chi_\parallel - \chi_\perp$ and deforms the helix. The free energy has to be in the constant amplitude approximation minimized with respect to $\phi(z)$ leading to the sine–Gordon equation:

$$\frac{d^2\phi}{dz^2} = \left(\frac{\chi_a H^2}{\tilde{K}_{33}}\right) \sin(2\phi) \qquad \text{(VII.2)}$$

which admits non–linear phase soliton solutions (i.e. a π–soliton lattice) for $H \neq 0$. Here $\tilde{K}_{33} = K_{33} - \epsilon\mu^2$. For $H > H_c$ the modulated structure is not stable and the system makes a transition into the homogeneously tilted Sm C phase. The Sm C*, Sm A and Sm C phases

coexist at the Lifshitz point which is given by

$$T_L = T_c + \frac{1}{\alpha}\epsilon C^2 + \frac{4}{\alpha}\frac{\tilde{\Lambda}^2}{\tilde{K}_{33}^2} \qquad \text{(VII.3a)}$$

$$H_L = 2\tilde{\Lambda}(\tilde{K}_{33}\chi_a)^{-1/2} \qquad \text{(VII.3b)}$$

The critical field for the unwinding of the helix as derived from (VII.2) in the constant amplitud approximation is

$$H_c = \frac{\pi}{4}H_L \qquad \text{(VII.4)}$$

Within the classical model H_c is temperature independent (Fig. 17a). Again the experiments[19] (Fig. 17b) do not follow the predictions of the above model. The critical field for the unwinding of the helix is strongly temperature dependent and allows for a reentrant Sm C* phase (Fig. 17b).

b) **In the presence of an electric field** E applied perpendicularly to the helical axis[20], a term

$$g_E = -EP_y$$

has to be added to the free energy density (III.5a). Minimizing the free energy with respect to the phase $\phi(z)$ one again obtains the sine-Gordon equation

$$\tilde{K}_{33}\theta^2\frac{d^2\phi}{dz^2} = \epsilon C\theta\cos\phi \qquad \text{(VII.5)}$$

which gives as a solution a 2π – soliton lattice. The period of this lattice goes to infinity (i.e. the helix unwinds) at a critical field

$$E_c = \frac{\pi^2}{16}\frac{\tilde{\Lambda}^2}{\tilde{K}_{33}\epsilon C}\theta \qquad \text{(VII.6)}$$

According to (VII.6) the temperature dependence of E_c should be the same as that of the tilt $\theta \propto (T_c - T)^{\beta}$. The experiments do not show such a temperature dependence of E_c. The measured E_c has

a non–monotonous T–dependence again leading to reentrant behaviour with varying temperature[20] (Fig. 18).

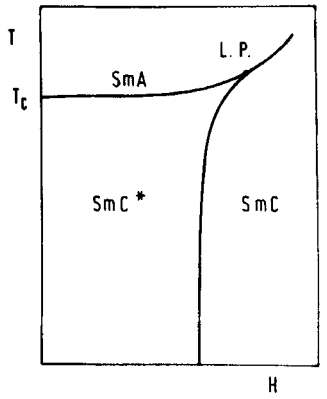

FIGURE 17a. Schematic phase diagram of a ferroelectric liquid crystal in external magnetic field as expected from the classical Landau model.

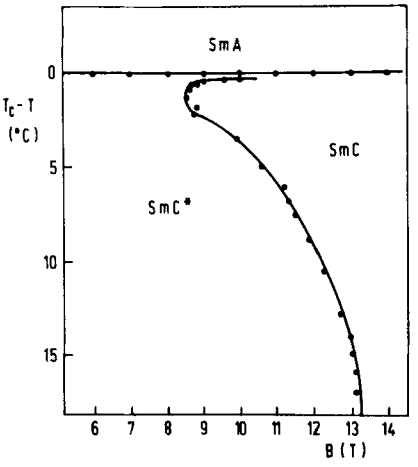

FIGURE 17b. Phase diagram of DOBAMBC in the external magnetic field applied perpendicularly to the helical axis

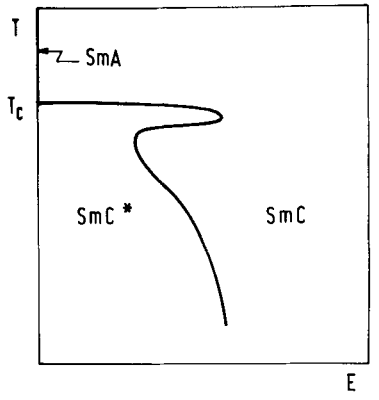

FIGURE 18. Schematic phase diagram of a ferroelectric liquid crystal in external electric field applied perpendicularly to the helical axis, drawn on the basis of experimental results. The Sm A phase exists only for $T > T_c$ and $E = 0$.

VIII. CHIRAL AND NON–CHIRAL TERMS IN THE FREE ENERGY DENSITY

The preceding survey of recent experimental data demonstrates that the classical Landau model of the Sm A – Sm C* transition fails to describe quantitatively some basic features of this transition though the observed values of the critical exponents show that within the experimentally accessible region the mean field approximation is correct. The most serious disagreements between the prediction of the classical theory[2,4] and existing experimental data are as follows:

i) The ratio between the polarization P and the tilt θ is a T–dependent quantity $P/\theta = f(T)$ and not a constant as predicted.

ii) The measured polarization in DOBAMBC and some other compounds displays $\cong$ 1 K below T_c an S–shaped T–dependence in contrast to the classical square root type dependence predicted by the model.

iii) The pitch of the helix, frequency of the phason mode and the critical magnetic field for the unwinding of the helix in an ex-

ternal transverse magnetic field are all T–dependent and not constant as predicted.

iv) The static dielectric constant does not show the predicted cusp at T_c but a broad maximum below T_c as given by eq. (VI.10).

v) The polar ordering around the long molecular axis observed in the Sm C^x phase is small compared to the bipolar (i.e. quadrupolar) one but there is no term in the classical free energy density to describe this effect.

All above effects were observed in this samples where the properties of the system do not depend anymore on the sample thickness.

To correct for the above deficiencies (i – iv), a generalized Landau model was developed[5,6,7,21] where the most essential thing is the introduction of a biquadratic coupling between the polarization and the tilt. This term which is of non–chiral character is far from T_c large compared to the bilinear coupling which is of chiral character. Thus a cross–over behaviour takes place from the regime close to T_c (where because of the smallness of θ only the bilinear coupling is important) to the regime far from T_c (where θ is large) and the biquadratic coupling dominates.

The main features of this generalized Landau model are presented in Fig. 19, and compared with the classical simplified theory and the corresponding experimental predictions. The generalized theory is capable of describing all the experimental features (i – iv).

It should be noticed that the biquadratic $\Omega\ (P_x \xi_2 - P_y \xi_1)^2$ term was first introduced by Žekš[5] whereas the sixth order term in the tilt was introduced independently by Huang and Viner[22] and by Carlsson and Dahl[7].

The new physics in the generalized model is the observation that chiral terms in ferroelectric liquid crystals are generally small as compared to non–chiral ones. That this is true can be seen from:

i) The small difference between the Sm A – Sm C^* transition temperature T_c in a ferroelectric liquid crystal and the corresponding Sm A – Sm C transition temperature of a racemic mixture of right and left handed compounds.

ii) The fact that the pitch of the helix is large as compared to the spacing of the smectic layers.

iii) The fact that the quadrupolar ordering of the transverse molecular axes induced by the tilt at both the Sm A – Sm C and the Sm A – Sm C* transition is large as compared to the polar ordering which is specific for Sm A – Sm C* systems.

The remaining open problem is the question why is the non–chiral biquadratic $\Omega P^2\theta^2$ term large as compared to the chiral bilinear C $P\theta$ term??

We believe that the origin of this effect is the presence of a hidden variable which does not explicitely appear in the generalized Landau model as presented in Fig. 19. This hidden variable is the biaxiality of the tilted smectic phases measuring the quadrupolar ordering of the transverse molecular axes, i.e. the bipolar biasing of the rotation around the long molecular axis:

$$\tilde{\eta}_1 \propto \frac{3}{2} \sin^2\theta_o \langle \cos 2\varphi \rangle \qquad \text{(VIII.1)}$$

as well as the asymmetry in the fluctuations of the long molecular axis

$$\tilde{\eta}_2 \propto \frac{3}{2} \langle \sin^2\beta \cos 2\phi \rangle \qquad \text{(VIII.2)}$$

The biaxiality is a result of both of these effects. In chiral systems we have an additional contribution namely the polar biasing of the rotation around the long axis:

$$\tilde{\eta}_3 \propto \sin 2\theta_o \langle \cos\varphi \rangle \qquad \text{(VIII.3)}$$

which is proportional to the tilt and not to the square of the tilt as $\tilde{\eta}_1$ and $\tilde{\eta}_2$.

The quadrupolar ordering $\tilde{\eta}_1$ and $\tilde{\eta}_2$ are proportional to the square of the tilt

$$\tilde{\eta}_{1,2} \propto \theta_o^2 \qquad \text{(VIII.4)}$$

SIMPLIFIED THEORY

Landau expansion of the free-energy density

$$g_0(z) = \frac{1}{2} a (\xi_1^2 + \xi_2^2) + \frac{1}{4} b (\xi_1^2 + \xi_2^2)^2 - \Lambda (\xi_1 \frac{d\xi_2}{dz} - \xi_2 \frac{d\xi_1}{dz}) +$$

$$+ \frac{1}{2} K_3 [(\frac{d\xi_1}{dz})^2 + (\frac{d\xi_2}{dz})^2] + \frac{1}{2\varepsilon} (P_x^2 + P_y^2) - \mu (P_x \frac{d\xi_1}{dz} + P_y \frac{d\xi_2}{dz}) + C (P_x \xi_2 - P_y \xi_1)$$

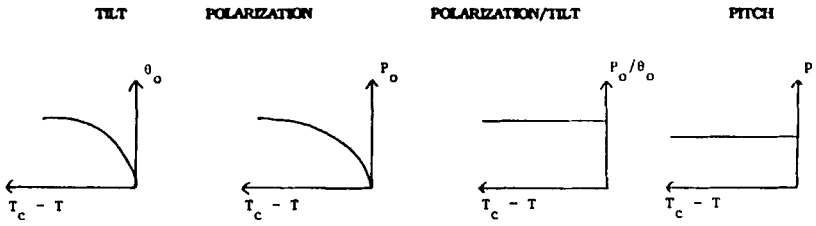

GENERALIZED LANDAU MODEL

$$g_0(z) = \frac{1}{2} a (\xi_1^2 + \xi_2^2) + \frac{1}{4} b (\xi_1^2 + \xi_2^2)^2 \boxed{+ \frac{1}{6} c (\xi_1^2 + \xi_2^2)^3} - \Lambda (\xi_1 \frac{d\xi_2}{dz} - \xi_2 \frac{d\xi_1}{dz}) +$$

$$+ \frac{1}{2} K_3 [(\frac{d\xi_1}{dz})^2 + (\frac{d\xi_2}{dz})^2] + \frac{1}{2\varepsilon} (P_x^2 + P_y^2) - \mu (P_x \frac{d\xi_1}{dz} + P_y \frac{d\xi_2}{dz}) + C (P_x \xi_2 - P_y \xi_1) -$$

$$\boxed{- \frac{1}{2} \Omega (P_x \xi_2 - P_y \xi_1)^2 + \frac{1}{4} \eta (P_x^2 + P_y^2)^2 - d (\xi_1^2 + \xi_2^2)(\xi_1 \frac{d\xi_2}{dz} - \xi_2 \frac{d\xi_1}{dz})}$$

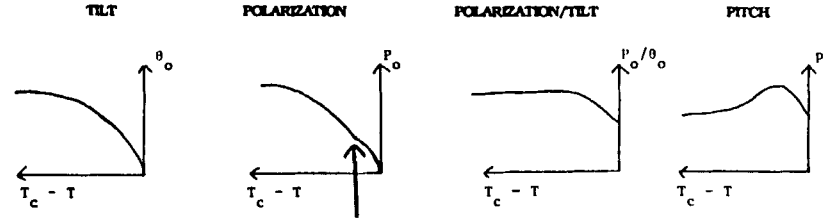

FIGURE 19. (a) Simplified theory: Landau expansion of the free-energy density. (b) Generalized Landau model.

and different from zero in the achiral Sm C as well as in the chiral Sm C* phases. They are also coupled to the square of the in–plane polarization in chiral systems. They are thus proportional to P^2 and responsible for the rather large achiral $P^2\theta^2$ term in the Sm C* phase.

REFERENCES

1. R.B. Meyer, L. Liebert, L. Strzelecki and P. Keller, J. Phys. (Paris), Lett. 36, L69 (1975).
2. V.L. Indenbom, S.A. Pikin and E.B. Loginov, Kristallografiya 21, 1093 (1976). (Sov. Phys. Crystallogr. 21, 632 (1976).
3. S. Dumrongrattana and C.C. Huang, Phys. Rev. Lett. 56, 464 (1986).
4. R. Blinc and B. Žekš, Phys. Rev. A 18, 740 (1978); R. Blinc, Phys. Stat. Sol. b 70, K29 (1975).
5. B. Žekš, Mol. Cryst. Liq. Cryst. 114, 259 (1984).
6. C.C. Huang and S. Dumrongrattana, Phys. Rev. A 34, 5020 (1986).
7. T. Carlsson and I. Dahl, Mol. Cryst. Liq. Cryst. 95, 373 (1983).
8. V.P. Shibaev, M. Kozlovsky, L.A. Beresnev, L.M. Blinov, and N.A. Plate, Polymer Bull. 12, 299 (1984).
9. S.T. Lagerwall and I. Dahl, Mol. Cryst. Liq. Cryst. 114, 151 (1984).
10. B.I. Ostrovskii, A.S. Rabinovicz, A.S. Sonin, B.A. Strukov and N.I. Czernova, Zh. Eksp. Teor. Fiz. Pisma Red 25, 80 (1977) (JETP Lett. 25, 70 (1977)); Ph. Martinot–Lagarde, J. Phys. (Paris) Lett. 38, L–17 (1977).
11. C.R. Safiniya, M. Kaplan, I. Als–Nielsen, R.J. Birgenau, D. Davidov and J.D. Litster, Phys. Rev. B 21, 4149 (1980); see also R.J. Birgenau et al., Phys. Rev. B 27, 1251 (1983).
12. S. Dumrongrattana, C.C. Huang, G. Nonmesis, S.C. Li and J.M. Viner, Phys. Rev. A 34, 5010 (1986).
13. R. Blinc, M. Luzar, J. Seliger, and V. Rutar, in "Liquid Crystals of One and Two–Dimensional Order", W. Helfrich, G. Heppke, Editors, Springer–Verlag Berlin (1980), p. 34; M. Luzar, V. Rutar, J. Seliger, and R. Blinc, Ferroelectrics 58, 115 (1984).

14. R. Blinc, M. Vilfan, and J. Seliger, Bull. Mag. Res. 5, 51 (1983).
15. A. Pines, M.G. Gibby, and J.S. Waugh, Chem. Phys. Lett. 15, 373 (1972); S. Pausak, A. Pines and J.S. Waugh, J. Chem. Phys. 59, 591 (1973); A. Pines, J.J. Chang and R.G. Griffin, J. Chem. Phys. 61, 1021 (1974).
16. I. Muševič and A. Seppen, to be published.
17. A. Levstik, T. Carlsson, C. Filipič, I. Levstik, and B. Žekš, Phys. Rev. A 35, 3527 (1987).
18. I. Muševič, A. Seppen, P. Wyder, R. Blinc, B. Žekš, C. Filipič, and A.P. Levanyuk, to be published.
19. I. Muševič, B. Žekš, R. Blinc, Th. Rasing, and P. Wyder. Phys. Rev. Lett. 48, 192 (1982); see also I. Muševič, B. Žekš, R. Blinc, L. Janssen, A. Seppen, and P. Wyder, Ferroelectrics 58, 71 (1984).
20. K. Kondo, H. Takezoe, A. Fukuda, and E. Kuze, Jap. J. Appl. Phys. 22, L43 (1983); S. Dumrongrattana and C.C. Huang, J. Physique 47, 2117 (1986) and references therein.
21. T. Carlsson, B. Žekš, C. Filipič, A. Levstik, and R. Blinc, Phys. Rev. A, to be published.
22. C.C. Huang and J.M. Viner, Phys. Rev. A 25, 3385 (1982).